

Bulk material influence on the aggressiveness of cavitation – Questioning the microjet impact influence and suggesting a possible way to erosion mitigation

Matevž Dular^{a,b,*}, Claus Dieter Ohl^b

^a Faculty of Mechanical Engineering, University of Ljubljana, Askerceva 6, 1000, Ljubljana, SI, Slovenia

^b Institute for Physics, Otto von Guericke University, Universitätsplatz 2, 39106, Magdeburg, DE, Germany

ARTICLE INFO

Keywords:

Cavitation
Bubble
Erosion
Material
Acoustic impedance

ABSTRACT

In a study conducted over 10 years ago (Petkovsek and Dular, 2013) [1] we noticed that the thin metal sheet sustains less cavitation damage when it is attached to an acrylic glass (PMMA) than in the case when we attached it to quartz glass (SiO₂). The reason for this was not explored at the time.

In the present paper we present a systematic study of single cavitation bubble erosion of a thin aluminum foil, which was attached to either PMMA or SiO₂ plate. We show that the damage sustained on the foil attached to PMMA plate is significantly smaller regardless of the bubble collapse distance from the boundary. The result is surprising since one would expect the weak foil to be severely damaged regardless of the material it is attached to.

By femtosecond illumination and high-speed image acquisition we were able to capture the formation and progression of the shock waves, which are emitted at cavitation bubble collapse and observed that they are reflected on SiO₂ boundary but that they traverse the PMMA bulk material. We offer an explanation that to achieve less damage the bulk material needs to have acoustic impedance similar to the one of the liquid medium in which cavitation occurs.

Further on, we constructed a simple composite material where PMMA was attached to the SiO₂ and showed that we can partially mitigate the damage. This was further confirmed by ultrasonic cavitation erosion tests.

The results also imply that the cavitation damage originates solely from the shock wave, which is emitted at cavitation bubble collapse – consequently putting the idea of microjet impact mechanism under question. Finally, the study offers a new exciting approach to mitigate cavitation erosion by fine tuning the acoustic impedance of the coatings.

1. Introduction

In brief, cavitation is the occurrence of vapor bubbles inside a liquid. It is known that in static conditions a liquid changes phase to vapor if its pressure is lowered below the so-called vapor pressure. In liquid flows, this phase change is generally due to local high velocities which induce low pressures. The liquid medium is then ruptured at one or several points and “voids” appear, whose shape depends strongly on the structure of the flow. The phenomenon is usually considered to be undesired since it can cause changes in flow dynamics, drop of efficiency or head of hydraulic machines, noise and also severe erosion of submerged surfaces. Cavitation and consequently cavitation erosion is one of the most

ubiquitous problems at operation of turbines, pumps, ship propellers and valves.

Cavitation erosion studies can be generally divided into three approaches which differ in the method that cavitation is generated. Usually, the effects of either hydrodynamic or acoustic (ultrasonic) cavitation on material is studied. Less common are the studies of single, laser generated, cavitation bubble collapse and the consequent damage (firstly observed as plastic deformation) appearance. Each of the methods has its advantages and issues. Most commonly and the easiest to use is acoustic cavitation, which yields results the fastest and has received standardization concerning its ability to erode material (ASTM G-32 standard [2]). However, the results from the standardized tests are

* Corresponding author. Faculty of Mechanical Engineering, University of Ljubljana, Askerceva 6, 1000, Ljubljana, SI, Slovenia.

E-mail address: matevz.dular@fs.uni-lj.si (M. Dular).

<https://doi.org/10.1016/j.wear.2023.205061>

Received 12 May 2023; Received in revised form 17 July 2023; Accepted 21 July 2023

Available online 27 July 2023

0043-1648/© 2023 The Authors. Published by Elsevier B.V. This is an open access article under the CC BY license (<http://creativecommons.org/licenses/by/4.0/>).

many times hard to apply to the “real” conditions, e.g. relating to cavitation in fast flows such as on ship propellers or pumps and in particular in the cases where protective coating is used. Hydrodynamic cavitation erosion tests are harder to perform and usually require large setups [3] but the results obtained by them relate best to the real application [4]. Also, here a standardized test, somewhat more demanding in terms of execution exists [5]. Finally, erosion studies from single cavitation bubbles reveal more physical insight into the process but cannot be easily used for direct material characterization [6–8].

Another way to distinguish cavitation aggressiveness studies is the means of evaluation. The straightforward approach is to measure the damage – either long term mass loss measurements [9,10] or merely determining the deformation of the surface (pit count) which can be performed after a much shorter period of exposure to cavitation [3, 11–13]. An alternative approach is to measure the pressure loads from the collapsing bubbles. Here miniature piezoceramic transducers are usually used. The experimental measurements of such impact loads using conventional pressure sensors are rarely reliable due to the micron size and the very small duration of the loading. A combination of the beforementioned approaches was introduced by Ref. [14] where numerous pits corresponding to localized plastically deformed regions were first identified, and each pit was then numerically reproduced by finite element simulations of the material response to a representative Gaussian pressure field supposed to mimic a single bubble collapse. This gave the size and pressure distribution of the bubble impacts.

The most common approach to improve the resistance of materials to cavitation erosion is to increase the hardness of the material surface by various methods (heat or thermo-chemical treatment, machining, cladding, laser processing, coating deposition ...) [15]. Usually the aim is straightforward – to increase the hardness of the surface [16]. Using softer coatings is less common. Here it is hypothesized that the surface firstly influences the cavitation behavior what consequently results in better protection of the bulk material [17,18]. Lately also composite [19, 20] and even memory shape materials [21,22] are being investigated for protection of machine parts against cavitation erosion.

The motivation for the present work comes from a study performed more than 10 years ago [1], where we, for the first time, simultaneously observed the dynamics of hydrodynamic cavitation and the damage (plastic deformation) occurrence on a thin metal sheet, which was attached to a venturi section beneath the vapor pocket. For the specific purpose of the measurements the Venturi needed to be transparent. Initially we used acrylic glass (PMMA) to manufacture it, but the damage was not detected. Eventually, we realized that the thin metal sheet (cavitation erosion sensor) needed to be attached to a Venturi section made of quartz glass (SiO_2) if the damage was to be detected after each cavitation event (for example cloud collapse). In Fig. 1 we show the

damage that was, during that study [1], collected on a thin aluminum foil attached to the wetted part of the SiO_2 glass and PMMA venturi and exposed to hydrodynamic cavitation for a period of 0.2 s.

Obviously one can see the difference in the damage on the PMMA and SiO_2 base when comparing the raw images of the foil (top and middle images in Fig. 1). While the aluminum foil, which was attached to the PMMA glass, remained almost undamaged, the one attached to a SiO_2 glass is locally severely deformed and even penetrated. The difference is even more obvious from the bottom two images, which show the difference between the raw images – no difference is detected for PMMA base, while plenty of pits can be seen (red) for SiO_2 case. The reason for this was not explored at the time these experiments were conducted, simply because the aim of the works different.

The same was found in our studies on single bubble cavitation erosion [7]. At that time a single cavitation bubble collapse and the damage occurrence was researched. Again, we concluded that the metal foil needs to be attached to a SiO_2 glass plate if the damage is to occur.

Actually, already in 1971 Hammit reports on the unusual response of plexiglas to cavitation erosion [23]. Also, acrylic glass was used to attenuate and to prevent reflection of the pressure wave in the design of cavitation impact load sensor after it was detected by piezoceramics [24].

The effect of the substrate material may seem obvious – it is well known that a softer substrate will better diffuse the elastic waves than a hard one [25], but in fact this is not the case. In those studies a very soft foil was attached to a substrate by an adhesive tape. The equivalent of the surface hardness is in the order of $\text{HV} = 0.4$ [1]. Hence one would expect it to get severely damaged regardless of the substrate beneath it. This was never the case – neither in hydrodynamic cavitation [1,26], nor in single bubble cavitation [7].

This study firstly repeats our previous investigations, where the effect of the substrate material was simply ignored as the aim was different, and then studies the interaction of the bubble with the material in a more detailed manner. The present study investigates the influence of the substrate material on the extent of cavitation erosion. We performed single bubble erosion experiments and visualizations of the bubbles together with the shock waves emitted. Then we discuss the reasons behind the results and question the importance of the microjet impact mechanism on the damage formation. Finally, by introducing “composite” (PMMA- SiO_2) bulk material we also offer a possibility that such an approach could be used for mitigation of cavitation erosion in turbomachinery, which we support by experiments on ultrasonic cavitation.

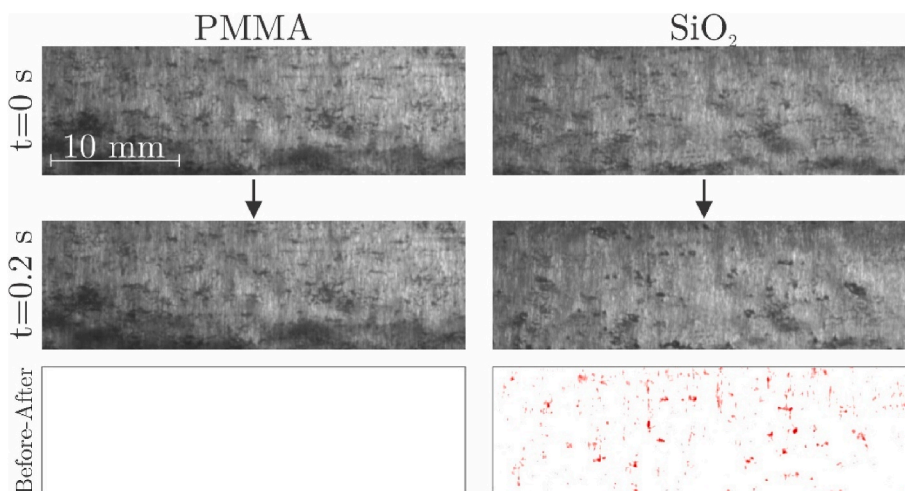


Fig. 1. Damage sustained after a short exposure ($t = 0.2\text{s}$) to hydrodynamic cavitation. A thin aluminum foil attached to the Venturi section is used as an erosion sensor. Left – the Venturi section is made of glass, right – the Venturi section is made of PMMA. Top images show the surface of the foil prior to experiment, middle show the foil after 0.2s exposure to cavitation and bottom show the difference between the two (in red). (For interpretation of the references to colour in this figure legend, the reader is referred to the web version of this article.)

2. Experimental set-up

2.1. Bubble generation

To study the phenomenon in detail, single bubble experiments were performed. These were prepared in a way that they enabled evaluation of the damage after a single bubble collapse, while they were also recorded with a high-speed camera. By using proper illumination, we could also detect the shock waves, which proved to be essential for the interpretation of the results. Fig. 2 shows the front and side view of the experimental setup.

Tests were performed as shown in the experimental setup sketched in Fig. 2. A single bubble (pos. 5) is generated in water in a glass cuvette (pos. 1) via optic cavitation with a pulsed laser (pos. 2) (Litron nano S, dimensions of cuvette approximately $50 \times 50 \times 80$ mm, focusing objective (pos. 4): Mitutoyo $50 \times$, numerical aperture $NA = 0.42$, nominal working distance: 20.5 mm, in-house modified with a water-tight sealing). The laser light pulse is beamed by a mirror (pos. 3) to the focusing objective (pos. 4), which is integrated into the cuvette bottom.

Images of the bubble were captured with a Shimadzu Hyper Vision HPV-X2 high speed video camera (pos. 8) at a framerate of typically 1,000,000 fps. The image resolution was 400×250 pixels ($8 \mu\text{m}/\text{pixel}$ resolution).

A mode-locked fiber-based femtosecond laser (pos. 9) (EXPLA FemtoLux 3, 515 nm wavelength) was used for backlight illumination. Approximately 300 fs long laser pulses were synchronized with the image acquisition such that a single laser pulse illuminated each frame. This technique allowed us to avoid all motion blurring and enabled the imaging of the shock waves.

The bubble reaches a maximum radius of about 1 mm. To avoid laser beam absorption at the solid boundary, as this would produce spurious bubbles or direct material ablation, the laser is focused parallel to the boundary. The distance of the laser focal point from the wall was always large enough to prevent clipping of the laser beam, which could affect bubble generation.

The focal point of the laser remained unchanged throughout the experimental campaign. The position of bubble collapse in respect to the erosion sensor (pos. 6) was adjusted in all 3 dimensions by precision positioning system (pos. 7).

Water quality is an issue in cavitating flow, but less so, when dealing with single bubble dynamics (when it is not extremely altered [27,28]). In the present study de-ionized water was used.

Each investigated condition (nondimensional distance) was repeated at least 5 times to gain a representative sample. After each lased breakdown the sample was moved for 5 mm to avoid superposition of

the pits.

2.2. Damage detection

The idea of the experiment was to observe the bubble collapse and the consequent damage on a thin aluminum foil which was attached to different bulk materials. Here we followed an approach from our previous studies [1,7,26] and used 1-mm-thick plates of SiO_2 or PMMA (25×75 mm) for the bulk (substrate). The thickness of the substrate did not influence the outcome of the results. At this dimension (1 mm) we could prevent any movement of the substrate and still visualize the shock wave on the back side of the glass (see Fig. 6).

A straightforward approach, which we tested already in 2013, would be to directly deposit a thin aluminum layer to the substrate. The issue is that then the surface is not comparably plastically deformable - the Al deposit is so thin that it cannot plastically deform without the influence of the material underneath it. The only type of damage that can occur in such an experiment is cracking and peeling of the Al layer. This is an issue since it cannot be compared between the experiments. Based this experience we used thin Al foil attached to adhesive tape, which is thick enough to allow deformation without interaction with the material it is attached to, making the results of experiments much more repeatable and independent of the structure beneath it.

The “damage sensor” (pos. 6 in Fig. 2 and in more detail in Fig. 3) was a 9- μm -thick aluminum foil which was attached to the glass plate by an optically clear two-sided adhesive tape with a thickness of 50 μm . This enabled optical measurement of the damage from both front and back side the foil was thin enough so that the cavitation damage, which occurs on the side exposed to cavitation bubble, was also visible on the other side. It must be noted here that holder for the plates was designed in a way to prevent its movement – this is especially critical in the case of PMMA plate, which exhibits a much more elastic behavior than SiO_2 plate.

Our reasoning is that we consider the aluminum foil attached to the adhesive tape as one material. Its properties were measured in our previous studies [1,7,26] – the equivalent (not according to standard) of

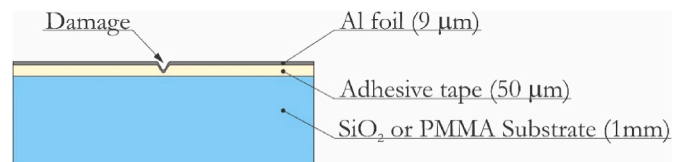


Fig. 3. The “construction” of the specimen.

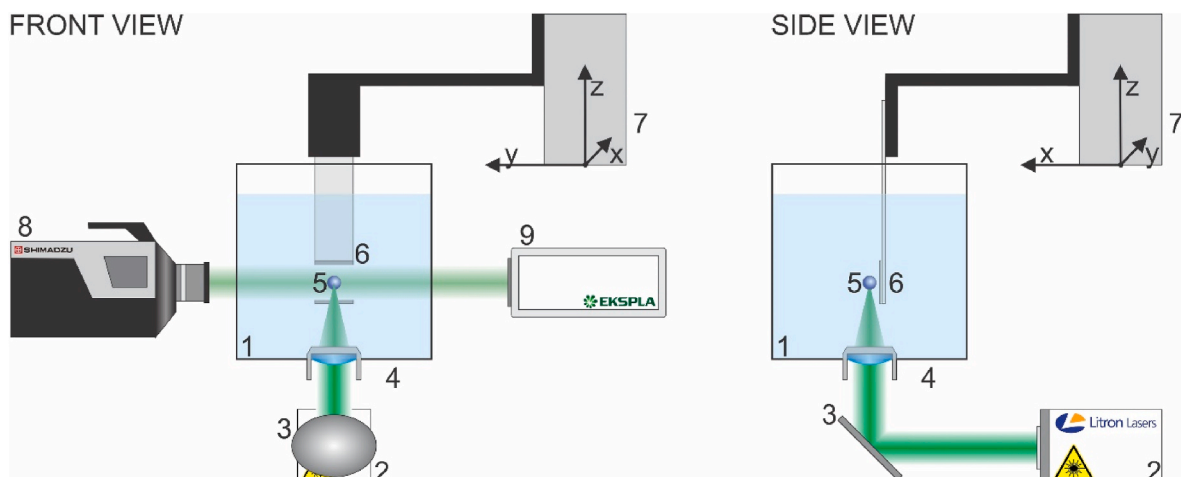


Fig. 2. Experimental set-up for single bubble collapse, shock wave and damage evaluation.

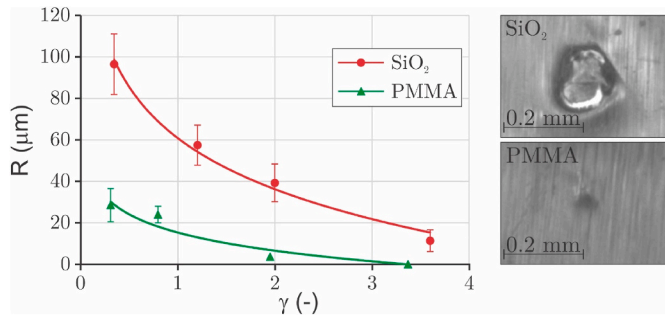


Fig. 4. Damage after bubble collapse at different nondimensional distances for different bulk materials (left). Typical appearance of a pit at $\gamma \approx 0.3$ for both materials.

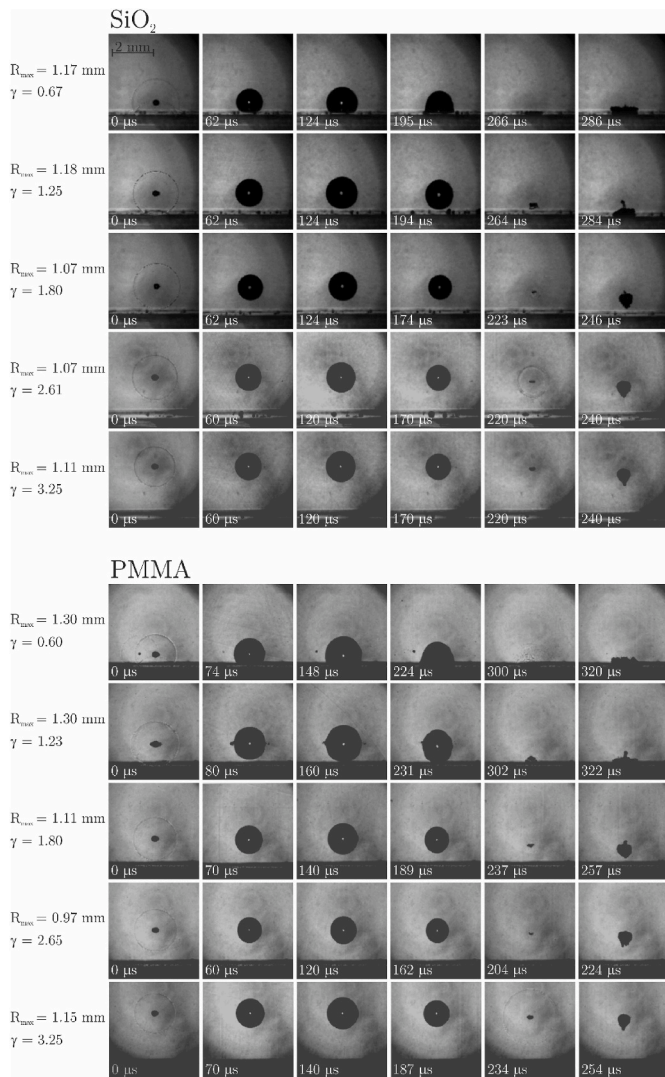


Fig. 5. Cavitation bubble collapse at different nondimensional distances for different bulk materials.

the surface hardness is in the order of $HV = 0.4$ [1]. Hence one would expect it to get severely damaged regardless of the substrate beneath it.

An essential reasoning for the present study is that the foils “will- ingness” to deform should be the same regardless of the substrate it is attached to. This was achieved by finding a sweet spot of foil and adhesive tape thickness.

The used approach makes the results of the present experiments

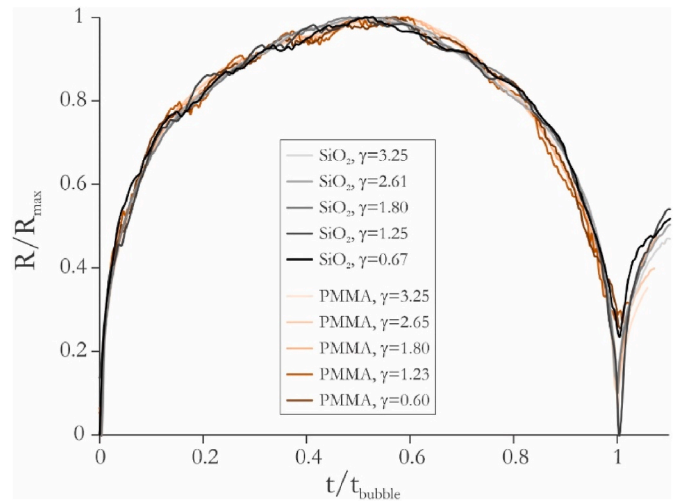


Fig. 6. Nondimensionalized bubble radius evolution for nondimensional distances and different bulk materials (corresponding to sequences in Fig. 5).

much more repeatable and independent of the structure beneath the foil and tape. As already mentioned, an alternative approach using direct aluminum deposition to the substrate proved inadequate as the durability varied for different substrate materials, cracking and peeling of the aluminum layer appeared and also the surface hardness varied for different substrates, making comparison overall impossible.

2.2.1. Damage evaluation

The present experiment setup could enable simultaneous recording of images of the cavitation bubble and the cavitation damage, as it was done in our previous study [1,7,26]. This was, however, not pursued. The damaged area was considered a parameter. The damage was evaluated by using a pit detection method, a simple yet reliable tool for estimation of cavitation aggressiveness [13]. From the comparison of the images of fresh and damaged surface, obtained with a microscope and a camera, we can recognize the changes - pits.

We evaluated the images prior and post exposure to cavitation bubble collapse – the intensity of every pixel of the image before the collapse was subtracted from the intensity of the same pixel after the collapse, what eliminated most of the surface and illumination imperfections.

Images of the aluminum foil were treated as matrices A with $i \times j$ elements $A(i,j) \in \{0,1, \dots, 255\}$ with 8-bit values which can range from 0 (black) to 255 (white). As mentioned, the damage was evaluated in image pairs: image matrix before the collapse (at time $t-1$) was subtracted from image matrix after the collapse (at time t): $B(i,j,t) = |A(i,j,t-1) - A(i,j,t)|$. Absolute value of the difference was used. This way a new matrix B was obtained. When the matrix element $B(i,j,t)$ did not change its value was $B(i,j,t) = 0$. When the change occurred, the value was $B(i,j,t) > 0$. Since small changes could be present due to insignificant changes in illumination, vibration etc., damage was only considered when a certain change threshold was exceeded (more than 5% of decrease or increase in brightness). The number of the pits, their size and overall damaged area could then be determined. More details on the methodology can be found in Ref. [1].

In the present study we focused on the damage that forms directly beneath the bubble – resulting from the microjet impact. The damage that occurred during the secondary evaporation and collapse (splashing) was not considered as it is much harder to detect and evaluate properly. Also, we have shown in Ref. [7] that in the presence of any deviation from the ideal conditions the damage after the secondary collapse does not appear. A typical case would be the presence of shear flow, to which a single cavitation bubble is subjected in any engineering application. Our reasoning was therefore to focus our observation on the damage

which forms at the microjet impact.

3. Results

First the results of the damage evaluation are shown. Comparison of cavitation bubble dynamics for different bulk materials follows. Finally, the results are discussed in terms of shock wave observation.

3.1. Damage

Fig. 4 shows the dependency of the average pit size in respect to the bulk material and in respect to the nondimensional distance of the bubble from the wall γ , defined as $\gamma = \frac{h}{R_{\max}}$ (h being the distance of the bubble center from the wall and R_{\max} the maximal radius of the bubble) Also typical pits for the case of SiO₂ and PMMA for the smallest distance - $\gamma \approx 0.3$ are presented.

We see that, regardless of the bulk material, the size of the pit increases rapidly as the bubble is created closer to the wall. Comparing this trend with the results from our past study with a similar setup [7] we can conclude that with the present damage evaluation approach (pit-count) we are only able to detect the deformation which originates from the microjet impact. Nonetheless this is a good enough indicator for comparison of the bulk material influence on the erosion process. Obviously, the properties of the bulk material to which the aluminum foil (erosion sensor) is attached to play a major factor in the erosion process. As already mentioned, the design of the plate holder prevented movement or bending of the plate during the experiment. Regardless of the nondimensional distance γ , the foil attached to PMMA plate sustained approximately 70% less damage compared to the foil attached to SiO₂. The result is surprising since one would expect the weak foil to be severely damaged regardless of the bulk material.

3.2. Bubble dynamics

Fig. 5 shows sequences of bubble collapse at different nondimensional distances from the solid surface; for different bulk materials (SiO₂ and PMMA glass).

The time evolutions vary slightly due to the influence of the nearby boundary and due to the slight size variations. The first image shown was taken 1 μ s after the optical breakdown. The second one at the mid time of bubble growth. The third one at the moment the bubble reached the maximal size. The fourth one at the mid time of the bubble collapse. The fifth one at the moment of bubble collapse. And the final one during the rebound, 20 μ s after the collapse.

By observing the bubble dynamics at the furthest distance from the boundary we can see that it follows the theoretical evolution relatively precisely – the theoretical Raileigh collapse time t_{col} can be estimated as [29]:

$$t_{\text{col}} = 0.918R \sqrt{\frac{\rho_l}{p - p_v}} \quad (1)$$

where R is the maximal bubble radius, ρ_l is the liquid density, p is the ambient pressure and p_v is the vapor pressure. Eq (1) gives 101 μ s compared to the measured 100 μ s for the most spherical 1.11 mm radius bubble $\gamma = 3.25$.

The control over the maximum bubble size was adequately achieved – staying in the order of $R_{\max} = 1.15$ mm. The nondimensional distance, from fully attached bubble at $\gamma = 0.60$ to a bubble relatively far away from the wall at $\gamma = 3.25$, are shown in Fig. 5. The experiments are grouped according to the material of the substrate beneath the bubble.

In the first images of the sequence one can clearly see the shockwave which resulted from the lased plasma discharge. In the case of the bubble in a close vicinity of the wall and SiO₂ ($\gamma = 0.67$) also a reflection of the shock wave can be seen. This is not the case for the corresponding case with PMMA substrate. This peculiarity is further examined later on. The

bubble collapses relatively spherically as long as γ is significantly larger than unity. In these cases, also a clear formation of the shockwave can be seen. There is no implication that it is not emitted even in the case of $\gamma < 1$, but it occurs on the surface itself and it therefore cannot be visualized.

In all cases the rebound is severely influenced by the presence of the solid surface - the bubble develops in the direction towards the wall. For $\gamma < 1$ also a clear case of “splashing” [30] can be seen.

As expected [31], the collapse time is longer for bubbles that implode closer to the boundary - in the case of $\gamma < 1$ the collapse time is about 30% too long, while it fits the theoretical much better when γ is larger.

Comparing the bubble topology dynamics between the two bulk materials we see that it does not change significantly when the material underneath it is changed. There are no topological changes and the small differences in the growth and collapse times (at a constant nondimensional distance) can be attributed solely to variations in the maximum size of the bubble. We can conclude from these observations that the bubble collapse rate as such cannot be the reason for the significant change in sustained damage of the foil attached to the SiO₂ and PMMA glass.

The repeatability and the influence of the substrate was further tested against the bubble apparent radius (the area of the bubble occupied in the image was measured. Then the equivalent bubble (sphere) radius was determined) evolution in time. The values in Fig. 6 are nondimensionalized against the apparent maximal bubble radius R_{\max} and the lifetime of the bubble t_{bubble} .

The apparent maximal bubble radius R_{\max} - the radius of a spherical bubble with a volume equivalent to the actual bubble volume. Obviously, we can observe that almost no difference for the value of γ and more importantly the substrate material can be seen when both the bubble radius and the time are nondimensionalized. Hence one can conclude that the outcome of the damage experiments are the result of the substrate material properties and not the influence of the substrate material on the bubble collapse itself.

A closer inspection of the images just before and right after the collapse revealed an important difference in the shock wave dynamics. The exposure time is 300 fs. The way this was achieved is that we opened the shutter of the camera for the full time of single frame (1 μ s in the case of 1Mfps acquisition) and synchronized the 300 fs bursts of the illumination laser with the frequency of camera acquisition. The shock is virtually frozen during this time. As we use shadowgraphy, the intensity in the image is formed by the second spatial derivative of the pressure. The shock wave width in the image is about 5 pixels, that would relate to width of 40 μ m (image resolution is 8 μ m/pixel, which is also the main source of uncertainty of this measurement) or a duration of 25ns assuming a velocity of 1500 m/s. Similar durations have been measured lately by Lokar et al. [32]. Unfortunately, the shockwaves are hardly visible in still images, but very clear in the movies – we invite the reader to find them among the supplementary files. Fig. 7 shows the two cases for $\gamma = 1.80$.

During the bubble collapse shock waves are emitted. At $\gamma = 1.80$ and $R_{\max} = 1.1$ mm the shock wave traveling with a velocity of about $c = 1480$ m/s takes slightly more than 1 μ s to traverse the distance from the bubble center to the wall. Its position is marked by yellow arrows in the second image of the series. Looking first at the case of SiO₂ glass (top series), a microsecond later the shock wave spreads to the radius of 3 mm (yellow arrows). In the same image one can also notice the shock wave reflection, which is marked by red arrows. The same continues later on – in the last image of the series, the primary shockwave (yellow arrows) spreads to 4.5 mm and the reflected one (red arrows) follows it with the same velocity.

As for the case of PMMA (bottom series), the primary shockwave behaves the same, but one cannot detect its reflection at the surface, which means that more of the energy is transported into the PMMA where it may be i) absorbed, ii) it simply passes it, or iii) the combination of the two.

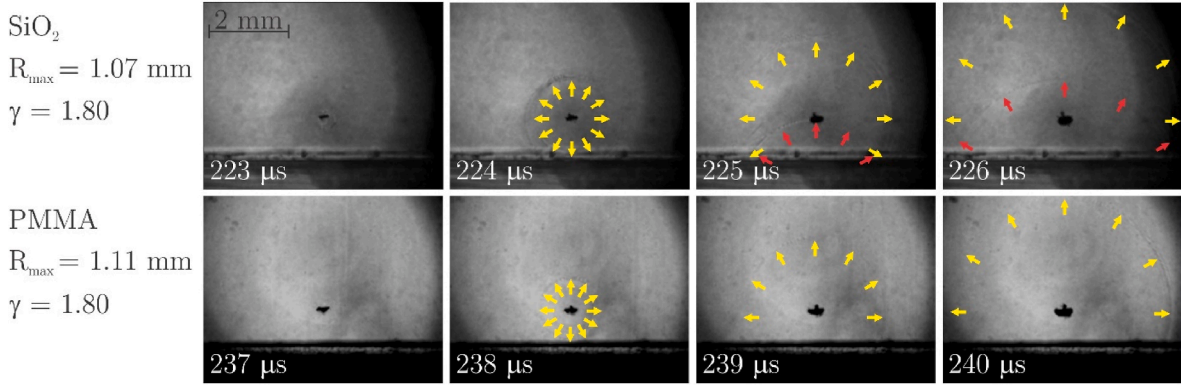


Fig. 7. Shock wave progression after the bubble collapse at $\gamma = 1.80$ for different bulk materials (top – SiO₂, bottom – PMMA).

4. Discussion

The ability of an interface to reflect an acoustic wave is related to the ratios of acoustic impedances of the two materials, i.e. that of water and PMMA or SiO₂. In fact, De & Hammitt [33,34] considered the importance of acoustic impedance when designing stems for detecting cavitation noise with further application to erosion prediction. They however did not make the transition to the idea to possibly use the impedance change for mitigation of erosion.

To estimate the reflection and the transmission coefficients one needs to consider the multilayer structure of the specimen. Here we adopt the approach commonly used in the design of ultrasonic transducers [35]. The acoustic impedance Z of individual material is defined as the product of the materials density ρ and the linear speed of the sound c [36]:

$$Z = \rho \cdot c \quad (2)$$

The characteristic impedances of the fluid, the layers of aluminum, the adhesive tape and the substrate are noted by Z_f , Z_{Al} , Z_t and Z_s , respectively. The thickness of the layers and the substrate material are t_{Al} , t_t and t_s , respectively. For a layer n of thickness t_n and acoustic impedance Z_n the transfer matrix is given by:

$$T_n = \begin{bmatrix} \cos \theta_n & jZ_n \sin \theta_n \\ \frac{j}{Z_n} \sin \theta_n & \cos \theta_n \end{bmatrix} \quad (3)$$

where θ_n represents the phase shifting equal to $\theta_n = \frac{2\pi t_n}{\lambda_n}$, with λ_n being the wavelength and t_n the thickness of the n -th layer (n being Al, t or s for aluminum foil, adhesive tape and substrate, respectively). Since the thickness of the substrate is much bigger than the other layers, one can define the equivalent resulting impedance Z_{eq} seen as:

$$Z_{eq} = \frac{T_{11}Z_s + T_{12}}{T_{21}Z_s + T_{22}} \quad (4)$$

where T_{ij} are the elements of the transfer matrix T resulting of the multilayered structure, defined by:

$$[T] = T_1 T_2 = \begin{bmatrix} T_{11} & T_{12} \\ T_{21} & T_{22} \end{bmatrix} \quad (5)$$

For a structure as presented in Fig. 3, the above transfer matrix is given by:

$$T_{11} = \cos \theta_{Al} \cos \theta_t - \frac{Z_{Al}}{Z_t} \sin \theta_{Al} \sin \theta_t \quad (6)$$

$$T_{12} = j(Z_t \cos \theta_{Al} \sin \theta_t + Z_{Al} \sin \theta_{Al} \cos \theta_t) \quad (7)$$

$$T_{21} = j \left(\frac{\sin \theta_{Al} \cos \theta_t}{Z_{Al}} + \frac{\cos \theta_{Al} \sin \theta_t}{Z_t} \right) \quad (8)$$

$$T_{22} = \cos \theta_{Al} \cos \theta_t - \frac{Z_t}{Z_{Al}} \sin \theta_{Al} \sin \theta_t \quad (9)$$

The reflection (R) and transmission (T) coefficients are then:

$$R = \left| \frac{Z_l - Z_{eq}}{Z_l + Z_{eq}} \right|^2 \quad (10)$$

and

$$T = 1 - R, \quad (11)$$

respectively. For the present experimental campaign, the material properties are given in Table 1 below.

Considering the data in Table 1 and Eqs. (2–11) we see that for the case of Water-SiO₂ the reflected shock wave will have an amplitude of 79% of the incipient one. In contrast the amplitude of the wave reflected from PMMA is only 66% of the initial one. This can be possibly used to interpret the significantly smaller damage on the PMMA base – more energy is either absorbed in the bulk material or more energy passes through the bulk material, while the thin foil attached to it remains less damaged. In the case of SiO₂ the energy is mainly absorbed by the thin foil attached to the glass, hence greater damage.

The above reasoning can also be qualitatively confirmed experimentally by shock wave visualization. Fig. 8 shows the observation of the initial shock wave which forms at optical breakdown. The time instant is 1.5 μ s after the breakdown (0.5 μ s after the first image in the series shown in Fig. 5). The above images show the visualization of the shock wave on the near side of the bubble and the bottom images show the visualization of the bubble on the far side of the bubble. The two images (near, far side) originate from separate experiments as it was impossible to record the shock wave on both sides of the SiO₂ (or PMMA) plate simultaneously.

Again, the yellow arrows point to the original shock wave and the red ones to its reflection at the boundary. A clear reflection can be seen for SiO₂, while none can be seen for PMMA. Looking at the bottom two images, to the far side of the plate we see that in the case of PMMA a somewhat weakened shock wave, which traversed the material with a

Table 1

Material and acoustic properties of the materials used in the experiment.

	ρ (kg/m ³)	c (m/s)	Z (kg/m ² s·10 ⁶)	t (m)
Water	1000	1480	1.48	∞
Al	2700	6400	17.2	0.000009
Adhesive	1160	1900	2.08	0.000050
SiO ₂	2200	5570	12.3	0.001
PMMA	1180	2680	3.16	0.001

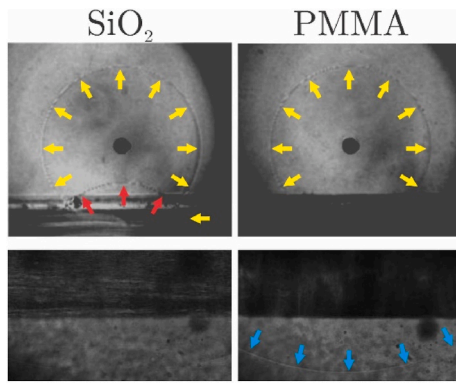


Fig. 8. Shock wave appearance 1.5 μ s after the optical breakdown (left – SiO₂, right– PMMA).

similar acoustic impedance as water, can be seen (blue arrows). None can be seen behind the SiO₂ plate.

4.1. Questioning the microjet impact theory

Currently, the most widely accepted explanation for the occurrence of cavitation erosion is that the potential energy contained in a macro cavity is transformed into the radiation of acoustic pressure waves, and further on into the erosive potential contained in single bubbles that collapse in the vicinity of the material boundaries [37,38]. Two theories describe the last stages of life of a micro-scale cavitation structure:

- The microjet [37]. For a bubble that forms near a rigid surface, due to the vicinity of the rigid surface, its upper boundary collapses faster than the one closer to the wall - a microjet forms. It can reach a velocity of several hundred m/s and as it hits the surface, which is high enough to deform the surface.
- Shock wave [39]. In the case of a spherical bubble collapse the formation of a shock wave seems obvious, but the shock wave is also emitted at asymmetric bubble collapse, when the microjet hits the bottom surface of the bubble as it was shown recently by Supponen et al. [40]. The amplitude of both is comparable and again high enough to cause material damage.

Going back to the microjet impact theory, Lush [41] suggested that it the case when the surface offers no resistance (which is a good enough approximation for the present experiment as the combination of the aluminum foil and adhesive tape is very soft) the material deformation velocity v_{def} is the same as the jet velocity v_{jet} . The deformation time t_{def} is related to the thickness (radius) of the jet r_{jet} and the sonic velocity in the liquid c_l . The depth of deformation d_{pit} would then be:

$$d_{pit} = v_{def} t_{def} = v_{jet} \frac{r_{jet}}{c_l} \quad (5)$$

By using common values of $v_{jet} = 100$ m/s, $r_{jet} = 0.1$ mm, we get $d_{pit} = 7$ μ m, which is in the same order of magnitude as reported in our previous study [7].

The above stated reasoning is the same for both the substrates, meaning that the extent of the damage should be comparable. However, the present experiments show that the damage extent is related to the impedance of the substrate material. This consequently implies that the foil was not damaged by microjet impact and puts the theory of erosion by microjet impact in question.

4.2. Path to erosion mitigation

Finally, we investigated the possibility of using a composite material – bonding SiO₂ as the carrier and PMMA as the absorber of the energy

(Al foil was attached to the PMMA plate via adhesive tape and this was then bonded to SiO₂ plate).

The reasoning was that the shock wave from the bubble collapse will be partially absorbed and will partially traverse the PMMA (as shown in Fig. 8 right). It will reach, at a much smaller amplitude, the SiO₂ plate where it will reflect (as shown in Fig. 8 left) just to be again absorbed in PMMA as it traverses it. On the bubble side of the plate, the shock wave dynamics should appear very similar to the case of using only PMMA plate.

Indeed, we found that a 1 mm thick PMMA “coating” prevents excessive damage to the surface of the material (Fig. 9).

In Fig. 9, essentially the diagram shown in Fig. 4, with an additional plot for the composite material, is shown. Again, for all three cases, one can see the strong dependence of the pit size on the bubble distance from the wall. In agreement with the previous finding, adding a sheet of PMMA on top of the SiO₂ plate significantly decreases the damage to the foil – approximately by 50% over the γ -range tested. This offers an exciting opportunity to mitigate cavitation erosion, using PMMA or other materials with acoustic impedance similar to waters for coatings of structures which usually suffer from cavitation damage (turbines, pumps, etc.). Still a scale up study should be performed. A step towards it is given in Fig. 8.

We performed a simple test of cavitation erosion by an ultrasonic horn. The procedure followed the ASTM G32 standard with a stationary specimen [2]. The specimens were prepared in the same way as for the single bubble tests. Since the aluminum foil is prone to be very quickly damaged by bubbles it was exposed to cavitation for only 1 s. The images of the damaged foil are shown in Fig. 10.

Here we present only the first trial test of cavitation erosion mitigation by a thin PMMA coating, hence the damage on the foil was only visually inspected (Fig. 10). One can obviously observe a significant decrease of the damage when the bulk material consisted of PMMA (right image). Despite the somewhat larger sustained damage, even more promising for the application, is the result of the damage on the composite bulk (middle image). Obviously, a coating by PMMA, influences the shock wave reflection also in the case of bubble cluster collapse.

Shima et al. [42] have utilized composite materials to deflect the bubble dynamics through elastic (rubber like) surface. Here, the rather stiff PMMA for cavitation mitigation does not affect the gross bubble dynamics and is therefore clearly different from their approach or that of Gonzalez et al. [43]. The PMMA substrate affects shock wave propagation not only during the expansion stage but also during the bubble collapses. The experiments here hint towards the possibility that the acoustic properties of the interface affect the final (here not resolved) stage of bubble collapse. We can only speculate, but it may very well be

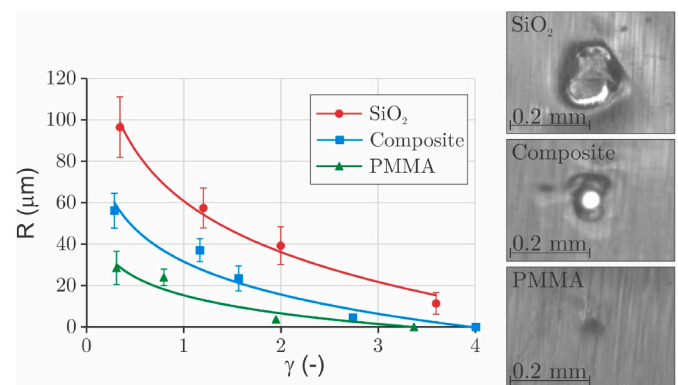


Fig. 9. Possible method for mitigation of erosion – use of composite material. Damage after bubble collapse at different nondimensional distances for different bulk materials (left). Typical appearance of a pit at $\gamma \approx 0.3$ for the 2 bulk materials and the SiO₂-PMMA composite.

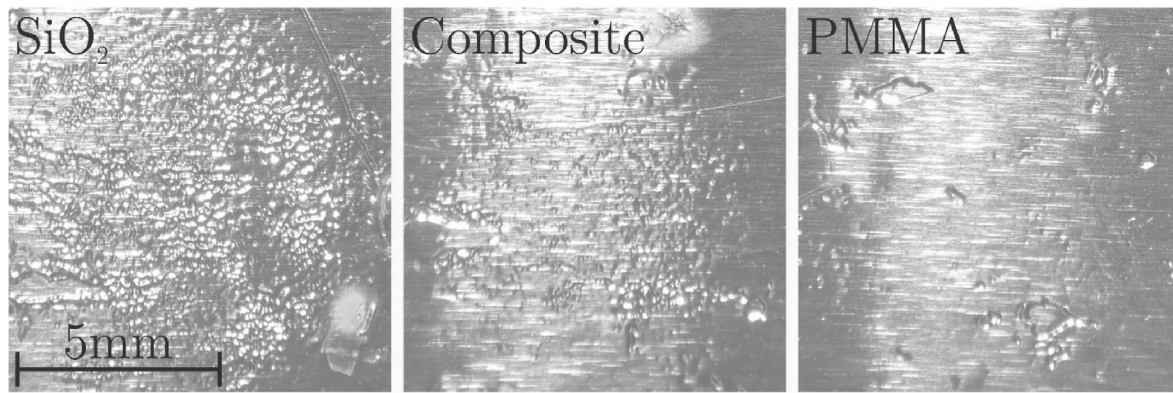


Fig. 10. Damage sustained by the foil attached to different bulk materials exposed to ultrasonic cavitation (ASTM G32 standard) for a period of 1 s.

that surface waves are essential for the final compression of the bubbles when generating erosion.

This offers a unique opportunity to investigate and develop coatings with appropriate acoustic impedance that would mitigate cavitation damage in turbomachinery. Of course, a much more detailed study needs to be performed to confirm this statement and surely many technical challenges (for example adhesion of the coating) will arise on the way.

5. Conclusions

While we have not fully resolved the mechanism that leads to cavitation damage, we have shown that the damage is strongly affected by acoustic impedance of the surface material. As smaller impedance, i.e. closer to impedance of the liquid medium (water), reduces the observed pit size and count (in the case of acoustic cavitation, Fig. 8). This may be an important step towards a new approach to cavitation erosion mitigation. Instead of focusing on elasticity of the coatings, which was thoroughly explored in the past, one could resolve on fine tuning the coatings acoustic impedance to prevent excessive damage to the bulk material.

In a recent work Reuter et al. [8] have shown that single laser induced bubbles cause damage at close distances and during the toroidal bubble collapse. There shock wave focusing rather than the microjet was the contributing factor for erosion. We may speculate that the particular acoustic property of the surface is decisive on the resulting damage.

Another, possibly more important observation of the present study is that the damage magnitude is related solely to the impedance of the substrate material, and this makes no sense if it is the water hammer pressure initiated by the microjet impact that causes the damage. Looking back to the work of Fortes-Patella et al., in 1998 [39] we see that she proposed the erosion to be the result of shock wave impact. This was questioned as it was believed that the magnitude of the shock wave emitted at jetting bubble collapse would be too small to cause damage. But in her study Supponen et al. [40,44] showed that it has almost the same magnitude as the one emitted from spherical collapse. The present results therefore imply that the microjet impact theory is in fact wrong. This could have major implication on the future development of cavitation erosion prediction models.

Further much more advanced studies with higher temporal and spatial resolution (on both bubble and material side) combined with measurement of longitudinal and transversal waves in the solid could help to connect the present measurements with the recent findings.

Declaration of competing interest

The authors declare that they have no known competing financial interests or personal relationships that could have appeared to influence the work reported in this paper.

Data availability

Data will be made available on request.

Acknowledgments

The authors acknowledge the financial support from the European Research Council (ERC) under the European Union's Framework Program for research and innovation, Horizon 2020 (grant agreement n 771567 – CABUM), the Slovenian Research Agency (Project No. J2-3057, Core funding No. P2-0422) and the support from the Humboldt Foundation Friedrich Wilhelm Bessel Research Award. The authors also thank dr. Fabian Reuter who designed and built the initial setup.

Appendix A. Supplementary data

Supplementary data to this article can be found online at <https://doi.org/10.1016/j.wear.2023.205061>.

References

- [1] M. Petkovšek, M. Dular, Simultaneous observation of cavitation structures and cavitation erosion, *Wear* 300 (2013), <https://doi.org/10.1016/j.wear.2013.01.106>, 1–2.
- [2] ASTM G32-16, *Standard Test Method for Cavitation Erosion Using Vibratory Apparatus*, ASTM International, West Conshohocken, PA, 2016.
- [3] G.L.C. Jean-Pierre Franc, Michel Riondet, Ayat Karimi, Material and velocity effects on cavitation erosion pitting, *Wear* 274–275 (Jan. 2012) 248–259, <https://doi.org/10.1016/j.WEAR.2011.09.006>.
- [4] Advanced experimental and numerical techniques for cavitation erosion prediction, in: K.-H. Kim, G. Chahine, J.-P. Franc, A. Karimi (Eds.), *Fluid Mechanics and its Applications*, vol. 106, Springer Netherlands, Dordrecht, 2014, <https://doi.org/10.1007/978-94-017-8539-6>, 106.
- [5] ASTM G134 : Standard Test Method for Erosion of Solid Materials by Cavitating Liquid Jet. https://global.ihs.com/doc_detail.cfm?document_name=ASTM%20G134&item_s_key=00234644 (accessed January. 3, 2023).
- [6] A. Philipp, W. Lauterborn, Cavitation erosion by single laser-produced bubbles, *J. Fluid Mech.* 361 (1998) 75–116, <https://doi.org/10.1017/S0022112098008738>.
- [7] M. Dular, T. Požar, J. Zevnik, R. Petkovšek, High speed observation of damage created by a collapse of a single cavitation bubble, *Wear* 418–419 (2019), <https://doi.org/10.1016/j.wear.2018.11.004>.
- [8] F. Reuter, C. Deiter, C.D. Ohl, Cavitation erosion by shockwave self-focusing of a single bubble, *Ultrason. Sonochem.* 90 (Nov. 2022), 106131, <https://doi.org/10.1016/j.ULTSONCH.2022.106131>.
- [9] G.L. Chahine, J.P. Franc, A. Karimi, Mass loss and advanced periods of erosion, *Fluid Mech. Appl.* 106 (2014) 97–121, <https://doi.org/10.1007/978-94-017-8539-6.5>.
- [10] A. Osterman, B. Bachert, B. Sirok, M. Dular, Time dependant measurements of cavitation damage, *Wear* 266 (9–10) (Apr. 2009) 945–951, <https://doi.org/10.1016/j.WEAR.2008.12.002>.
- [11] M. Dular, O.C. Delgosa, M. Petkovšek, Observations of cavitation erosion pit formation, *Ultrason. Sonochem.* 20 (4) (2013), <https://doi.org/10.1016/j.ultsonch.2013.01.011>.
- [12] J.P. Franc, G.L. Chahine, A. Karimi, Pitting and incubation period, *Fluid Mech. Appl.* 106 (2014) 37–69, <https://doi.org/10.1007/978-94-017-8539-6.3>.

- [13] M. Dular, B. Bachert, B. Stoffel, B. irok, Relationship between cavitation structures and cavitation damage, *Wear* 257 (11) (2004), <https://doi.org/10.1016/j.wear.2004.08.004>.
- [14] S.C. Roy, J.P. Franc, M. Fivel, Cavitation erosion: using the target material as a pressure sensor, *J. Appl. Phys.* 118 (16) (Oct. 2015), <https://doi.org/10.1063/1.4934747>.
- [15] A.K. Krella, Degradation and protection of materials from cavitation erosion: a review, *Materials* 16 (5) (Mar. 2023), <https://doi.org/10.3390/MA16052058>.
- [16] A.K. Krella, Cavitation erosion resistance parameter of hard CAVD coatings, *Prog. Org. Coating* 70 (4) (Apr. 2011) 318–325, <https://doi.org/10.1016/j.PORGCOT.2010.11.013>.
- [17] J.H. Lee, K.J. Lee, H.G. Park, J.H. Kim, Possibility of air-filled rubber membrane for reducing hull exciting pressure induced by propeller cavitation, *Ocean. Eng.* 103 (May 2015) 160–170, <https://doi.org/10.1016/j.OCEANENG.2015.04.073>.
- [18] S. Cao, G. Wang, O. Coutier-Delgosha, K. Wang, Shock-induced bubble collapse near solid materials: effect of acoustic impedance, *J. Fluid Mech.* 907 (2021) A17, <https://doi.org/10.1017/JFM.2020.810>.
- [19] G. Taillon, S. Saito, K. Miyagawa, C. Kawakita, Cavitation erosion resistance of high-strength fiber reinforced composite material, *IOP Conf. Ser. Earth Environ. Sci.* 240 (6) (Mar. 2019), 062056, <https://doi.org/10.1088/1755-1315/240/6/062056>.
- [20] R. Guobys, Rodríguez, L. Chernin, Cavitation erosion of glass fibre reinforced polymer composites with unidirectional layup, *Compos. B Eng.* 177 (Nov. 2019), <https://doi.org/10.1016/j.COMPOSITESB.2019.107374>.
- [21] S. Hattori, A. Tainaka, Cavitation erosion of Ti-Ni base shape memory alloys, *Wear* 262 (1–2) (Jan. 2007) 191–197, <https://doi.org/10.1016/j.WEAR.2006.05.012>.
- [22] T. Volkov-Husović, et al., Microstructural and cavitation erosion behavior of the CuAlNi shape memory alloy, *Metals* 11 (7) (Jun. 2021) 997, <https://doi.org/10.3390/MET11070997>, 2021, Vol. 11, Page 997.
- [23] F.G. Hammitt, *Cavitation Erosion State of Art and Predicting Capability*, 1979. Michigan.
- [24] T. Okada, S. Hattori, M. Shimizu, A fundamental study of cavitation erosion using a magnesium oxide single crystal (intensity and distribution of bubble collapse impact loads), *Wear* 186–187 (Aug. 1995) 437–443, [https://doi.org/10.1016/0043-1648\(95\)07162-8](https://doi.org/10.1016/0043-1648(95)07162-8).
- [25] J.D. Achenbach, *Wave Propagation in Elastic Solids*, Elsevier Science Publishers, 1975.
- [26] M. Dular, M. Petkovsek, On the mechanisms of cavitation erosion - coupling high speed videos to damage patterns, *Exp. Therm. Fluid Sci.* 68 (2015), <https://doi.org/10.1016/j.expthermfluidsci.2015.06.001>.
- [27] A. Jayaprakash, S. Singh, G.L. Chahine, Experimental and numerical investigation of single bubble dynamics in a two-phase bubbly medium, *ASME J. Fluid Eng.* 133 (12) (2011), 121305-1-121305-9.
- [28] J. Ma, G.L. Chahine, C. Hsiao, Spherical bubble dynamics in a bubbly medium using an Euler – Lagrange model, *Chem. Eng. Sci.* 128 (2015) 64–81, <https://doi.org/10.1016/j.ces.2015.01.056>.
- [29] J.P. Franc, J.M. Michel, *Fundamentals of Cavitation*, no. 1, Kluwer, Dordrecht, 2004, <https://doi.org/10.1007/s13398-014-0173-7.2>.
- [30] R.P. Tong, W.P. Schiffers, S.J. Shaw, J.R. Blake, D.C. Emmony, The role of 'splashing' in the collapse of a laser-generated cavity near a rigid boundary, *J. Fluid Mech.* 380 (Feb. 1999), <https://doi.org/10.1017/S0022112098003589>.
- [31] F. Reuter, Q. Zeng, C.D. Ohl, The Rayleigh prolongation factor at small bubble to wall stand-off distances, *J. Fluid Mech.* 944 (Aug. 2022) A11, <https://doi.org/10.1017/JFM.2022.475>.
- [32] Ž. Lokar, D. Horvat, J. Petelin, R. Petkovšek, Ultrafast measurement of laser-induced shock waves, *Photoacoustics* 30 (Apr. 2023), <https://doi.org/10.1016/J.PACS.2023.100465>.
- [33] M.K. De, F.G. Hammitt, Instrument system for monitoring cavitation noise, *J. Phys. E* 15 (7) (Jul. 1982) 741–745, <https://doi.org/10.1088/0022-3735/15/7/012>.
- [34] M.K. De, F.G. Hammitt, New method for monitoring and correlating cavitation noise to erosion capability, *J. Fluid Eng.* 104 (4) (Dec. 1982) 434–441, <https://doi.org/10.1115/1.3241876>.
- [35] D. Callens, C. Bruneel, J. Assaad, Matching ultrasonic transducer using two matching layers where one of them is glue, *NDT E Int.* 37 (8) (Dec. 2004) 591–596, <https://doi.org/10.1016/j.ndteint.2004.03.005>.
- [36] K. Ohtani, T. Ogawa, Expansion wave and cavitation bubble generation by underwater shock wave reflection from the interface, *J. Mech. Eng.* 3 (6) (2016) 16–298, <https://doi.org/10.1299/MEJ.16-00298>.
- [37] M. Dular, B. Stoffel, B. irok, Development of a cavitation erosion model, *Wear* 261 (5–6) (2006), <https://doi.org/10.1016/j.wear.2006.01.020>.
- [38] J.T. Bark, G. J. Friesch, G. Kuiper, Ligtelijn, *Cavitation erosion on ship propellers and rudders*, in: 9th Symposium on Practical Design of Ships and Other Floating Structures, Luebeck-Travemuende Germany, 2004.
- [39] R.F. Patella, J.L. Reboud, A new approach to evaluate the cavitation erosion power, *J. Fluid Eng.* 120 (2) (Jun. 1998) 335–344, <https://doi.org/10.1115/1.2820653>.
- [40] O. Supponen, D. Obreschkow, P. Kobel, M. Tinguely, N. Dorsaz, M. Farhat, Shock waves from nonspherical cavitation bubbles, *Phys Rev Fluids* 2 (9) (Sep. 2017), 093601, <https://doi.org/10.1103/PhysRevFluids.2.093601>.
- [41] P.A. Lush, Impact of a liquid mass on a perfectly plastic solid, *J. Fluid Mech.* 135 (1983) 373–387, <https://doi.org/10.1017/S0022112083003134>.
- [42] A. Shima, Y. Tomita, D.C. Gibson, J.R. Blake, The growth and collapse of cavitation bubbles near composite surfaces, *J. Fluid Mech.* 203 (199) (1989) 199–214, <https://doi.org/10.1017/S0022112089001436>.
- [43] S.R. Gonzalez-Avila, D.M. Nguyen, S. Arunachalam, E.M. Domingues, H. Mishra, C. D. Ohl, Mitigating cavitation erosion using biomimetic gas-entrapping microtextured surfaces (GEMS), *Sci. Adv.* 6 (13) (2020) 6192–6219, https://doi.org/10.1126/SCIADV.AAX6192/SUPPL_FILE/AAX6192_SM.PDF.
- [44] O. Supponen, D. Obreschkow, M. Tinguely, P. Kobel, N. Dorsaz, M. Farhat, Scaling laws for jets of single cavitation bubbles, *J. Fluid Mech.* 802 (Sep. 2016) 263–293, <https://doi.org/10.1017/jfm.2016.463>.